FERMILAB-PUB-08-515-E

Silicon Beam Telescope for LHC Upgrade Tests

T. Mäenpää [a] P. Luukka [a] B. Betchart [b] S. Czellar [a] R. Demina [b] Y. Gotra [b] M. Frey [c] F. Hartmann [c] J. Härkönen [a] S. Korjenevski [b] M.J. Kortelainen [a] T. Lampén [a] B. Ledermann [c] V. Lemaitre [d] T. Liamsuwan [c] O. Militaru [d] H. Moilanen [a] H.J. Simonis [c] L. Spiegel [e] E. Tuominen [a] E. Tuovinen [a] J. Tuominiemi [a]

[a] *Helsinki Institute of Physics, Helsinki, Finland*
[b] *University of Rochester, Dept. of Physics and Astronomy, Rochester, NY, USA*
[c] *Universität Karlsruhe (TH), Institut für Experimentelle Kernphysik, Karlsruhe, Germany*
[d] *Université catholique de Louvain, Louvain-la-Neuve, Belgium*
[e] *Fermi National Accelerator Laboratory, Batavia, IL, USA*

Abstract

A beam telescope based on the CMS Tracker data acquisition prototype cards has been developed in order to test sensor candidates for S-LHC tracking systems. The telescope consists of up to 8 reference silicon microstrip modules and slots for a couple of test modules. Beam tracks, as measured by the reference modules, provide a means of determining the position resolution and efficiency of the test modules. The impact point precision of reference tracks at the location of the test modules is about 4 μm. This note presents a detailed description of the silicon beam telescope (SiBT) along with some results from its initial operation in summer 2007 in the CERN H2 beamline.

1. Introduction

Silicon pixel and microstrip detectors are widely used in particle physics experiments due to their excellent spatial resolution and well-established manufacturing technology. In modern high-energy physics (HEP) experiments, however, the radiation environment is very hostile towards silicon detectors. Radiation-induced defects in the silicon sensors lead to an increase in leakage current, a decrease in charge collection efficiency (CCE) due to the trapping of charge carriers, and a change in the effective doping concentration. For n-type silicon the latter may lead to type inversion or, as it is more accurately described, Space Charge Sign Inversion (SCSI). If irradiation continues after SCSI, the voltage required for full depletion will steadily increase with increasing fluence. Radiation hardness up to 2×10^{15} 1 MeV n_{eq}/cm^2 is required for the sensors in the innermost silicon strip tracker layers of the planned Super-LHC (S-LHC) detectors. At the fluences exceeding 1×10^{15} 1 MeV n_{eq}/cm^2 the voltage required for full depletion of 300 μm thick sensors exceeds any practically available bias voltages, and at the same time more than 50% of the particle generated charge is trapped [1]. Clearly, more robust solutions will need to be identified for S-LHC.

Since the 1990's, a considerable amount of research has gone into improving the radiation hardness of silicon detectors. The developed approaches range from using magnetic Czochralski (MCz) silicon [2] to operating the devices at cryogenic temperatures [3], and to designing special detector structures such as p-type [4] or semi-3D detectors [5]. In order to demonstrate that the new detector technologies are suitable for large scale tracker systems, it is necessary to perform extensive tests on segmented sensors with a full readout chain.

The CCE of a sensor is a product of trapping and a geometrical factor related to the full depletion. In

other words, it is partly determined by the electric field distribution in silicon, which in irradiated silicon is complicated and exhibits, for example, a so-called double junction (DJ) structure [6]. Moreover, the electric field distribution depends on the segmentation of the sensor. In segmented sensors the holes (or electrons) generated by a traversing particle do not uniformly induce charge throughout the detector volume as is the case for diodes, but rather induce increasingly larger charges the closer they are to a segmented electrode [7]. Thus, higher charge collection is expected in segmented detectors than in diodes, which have been used in the majority of the irradiation hardness studies so far. Furthermore, SCSI can also affect charge collection efficiency. Despite extensive research, the SCSI phenomenon, for example, in MCz silicon is poorly understood and it is still an open question whether this occurs in n-type MCz silicon [8,9]. However, it is assumed that SCSI will manifest itself as a degradation in cluster resolution after the anticipated point of type inversion. Thus, to fully characterize candidate materials for radiation hard detectors it is necessary to measure cluster resolution, signal-to-noise, and charge collection efficiency of segmented devices made of these materials. These parameters are essential for position sensitive detectors, and their measurement was the motivation for the the Silicon Beam Telescope (SiBT) [10,11] and the subsequent upgrade of the system in 2007.

The upgrade of the earlier SiBT was necessary as the efficiencies of the sensors of the reference telescope had deteriorated to an unacceptable level. In the new design other issues such as cooling and integration time of the readout electronics were also addressed. The design followed the principles of the previous system. In the LHC experiments the resolution of the tracking sensors has to be 10–20 micrometers and the efficiencies close to 100% to achieve the aimed resolution of the momentum measurement in the tracker. Hence to check these parameters of a sensor to be tested, the reference telescope should achieve an impact point resolution considerably better than that. To measure the efficiency of the telescope itself one needs a minimum of four space points. This is most straightforwardly achieved by two sets of 4 modules, where one set is orthogonal to the other.

In order to test the sensors at the temperatures used in the tracking devices of the LHC experiments, the new telescope was installed inside a cold chamber known as the Vienna box, which was originally used for temperature cycling tests of the CMS Tracker silicon detector modules. The box contains 10 slots for modules with a 4 cm separation between slots. In the SiBT application 8 of the slots are reserved for reference detectors and 1–2 middle slots are reserved for detectors under study. Although the 4 cm spacing was originally intended to provide adequate ventillation during module burn-in, it also provides a sufficent lever-arm for reference tracking.

As described in references [12,13], the shaping time of the detector readout electronics affects the measured shot noise. That is, a long readout chip shaping time results in higher shot noise. This can be detrimental when studying irradiated detectors because in the irradiated sensors the reverse current shot noise is much higher than in the non-irradiated devices. For this reason the SiBT was upgraded in 2007 from a detector readout based on the VA1 chip (Ideas ASA, Norway), which has a 1 μs shaping time, to a readout based on the CMS (Compact Muon Solenoid) Tracker data acquisition APV [14,15] IC, which has the shaping time of about 50 ns.

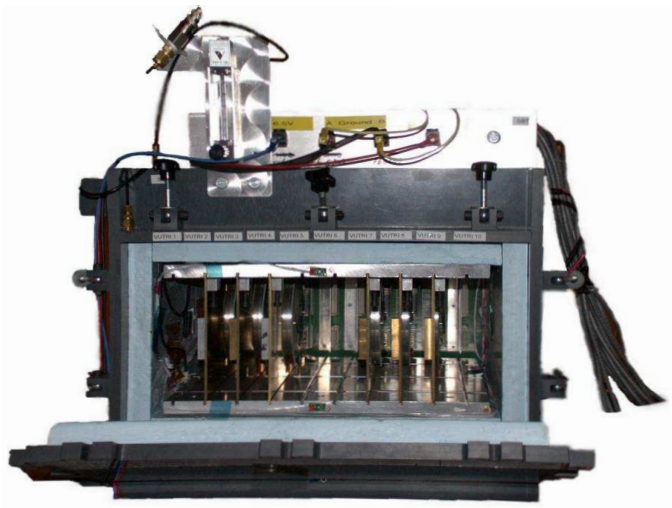

Fig. 1. A CMS long-term module test chamber (Vienna box) was used to position up to 10 modules in the test beam. The chamber provides both temperature and humidity control and additionally shields the biased modules from light. The width of the Vienna box is 60 cm.

2. Mechanics and Cooling

The SiBT detectors are housed inside the Vienna box. The box temperature is set by two water-cooled 350 W Peltier elements, which are in thermal con-

tact with the floor and ceiling of the inner chamber. Nitrogen is circulated in the box in order to avoid condensation. Without any internal load the box temperature can in principle be set as low as $-30\,^{\circ}$C and as high as $+70^{\circ}$C. During summer 2007 beam tests, where 9 modules (54 APV's) were operated simultaneously, the box was operated in the temperature range of $-20\,^{\circ}$C to $0\,^{\circ}$C.

The power consumption of each APV hybrid is approximately 2 W, depending on the APV configuration [14]. The power is regulated by the VUTRI cards which in turn are powered by standard laboratory supplies. Heat generated by the APV's in the thermally insulated Vienna box needs to be removed through active cooling. However, due to a well known weakness [16] with the Phase Locked Loops (PLL's), some of the CMS hybrids temporarily stopped functioning when maximal cooling was applied (reaching an ambient temperature of$-20\,^{\circ}$C within the Vienna box). Therefore only 90 % of the maximal cooling power was used, resulting in slightly higher operating temperatures. This limitation will be overcome in future runs by including PLL reset commands in the startup sequence.

The detectors are connected to brass support plates, which allow quick insertion of the detectors into the Vienna box (Fig. 1). Brass was chosen to avoid binding with the aluminum plates of the box at very cold temperatures. Each slot is equipped with backplane connectors compatible with CERN-made VUTRI [17] adaptors and 30 pin auxiliary modules. There is a separate connector for reading out the temperature probes inside the Vienna box. Air temperature, both inside and outside of the Vienna box, as well as the temperatures of the surface plates in contact with the Peltier elements were monitored and logged. The temperature of the hybrids can be read and logged by the Data Acquisition (DAQ) system by reading the Detector Control Unit (DCU) chips [18] mounted on the hybrids.

3. Detectors

The reference sensors used in the SiBT are single-sided AC-coupled silicon strip detectors fabricated by Hamamatsu Photonics (HPK). These high resistivity float zone sensors have a specified thickness of $320\pm20\,\mu$m. The detectors contain 639 active strips on a $60\,\mu$m readout pitch [19]. The width of the strip implantation is $8\,\mu$m and there is a $2\,\mu$m wide metal overhang. The sensors also feature an electrically

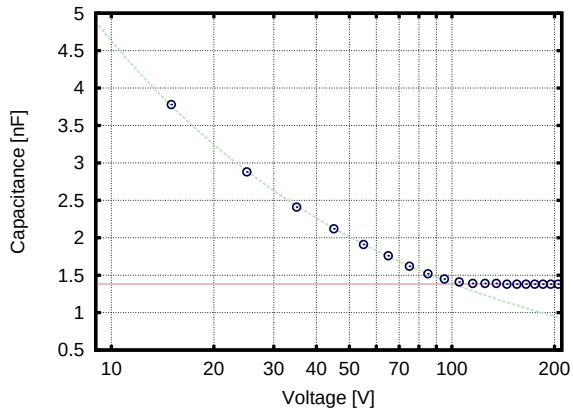

Fig. 2. CV measurement for DØ sensor L2-799. The capacitance saturation value is 1.38 nF, which corresponds to an effective thickness of $288\,\mu$m given the active area and pitch of the sensor. The average full depletion voltage of the DØ sensors was 111 ± 7 V, where the error represents the standard deviation of 12 V_{fd} values.

floating intermediate strip between active strips, so, as will be seen, the effective readout pitch is $30\,\mu$m. The active area of the reference detectors is approximately 98×38 mm^2. The full depletion voltage (V_{fd}) of the 12 detectors chosen for SiBT was measured by capacitance voltage (CV) method. A representative CV plot is shown in Fig. 2.

For the summer 2007 beam studies the reference detectors were biased with 150 V by CAEN SY127 power supplies. The total leakage current, measured at the room temperature, was less than 300 nA in all sensors. These sensors had been purchased by the DØ experiment for the proposed Run IIb at the Fermilab Tevatron.

In the summer 2007 beam studies slot six of the Vienna box was reserved for the detector under test (DUT), as shown in Fig. 3. Slots 1–3, 5, and 7–10 were then populated with reference modules. In Fig. 3 "+" refers to a module with a +45 orientation relative to the floor of the box and "−" to a −45 degree orientation. A 90 degree rotation, which would have been preferred, was not possible due to the tight clearance height of the Vienna box.

The HPK sensors were connected to CMS APV hybrid boards [14,20] via pitch adapters made at MINFAB [1]. The hybrids used in the SiBT were the Tracker Outer Barrel (TOB) versions with six APV25 chips. Since each APV chip comprises 128

[1] Micro- and Nanofabrication Centre, Helsinki University of Technology, Finland.

readout channels, the 639 reference detector strips were read by the first 5 APV's on the hybrids.

The APV hybrids are connected to readout electronics through VUTRI adaptors and VUTRI cards. The VUTRI adaptors are placed inside the Vienna box; VUTRI cards are placed outside.

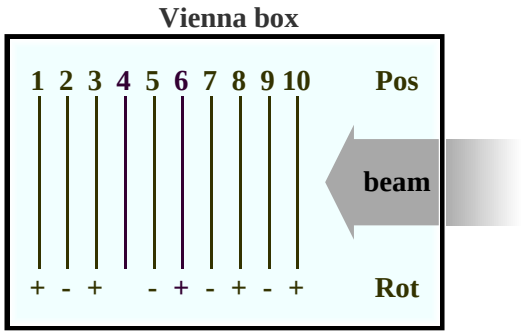

Fig. 3. The position and orientation of each detector in the summer 2007 test runs. Slot 6 contained the detector under study; slot 4 was not used. The + and − signs refer to ± 45° rotations of the modules. The hybrids of the + detectors were pitched upward in the box and the − detector hybrids were low. The detectors were normal to the beam.

4. Trigger

The CMS APV runs in a synchronous mode and requires the presence of a clock signal. In the 2007 runs a Trigger Sequencer Card (TSC) [21] was used to generate a local clock and the DAQ was synchronized to this. Particles in the SPS beam in the 2007 runs were asynchronous with the local 40 MHz SiBT master clock. This meant that when APV hybrids sampled their inputs into the internal ring buffer, the signal level was not always at its peak value. Since the APV's were operated in *peak mode*, which has a more generous time sampling, the estimated loss in signal due to the asynchronous nature of the beam was about 10%. Signal loss could have been avoided by gating the trigger so that it accepted only those particles that are coincident with the master clock. The gate width is tunable, with a granularity of about 1 ns [21]. This approach would have maximized signal size at the cost of a reduced trigger rate. The clocking arrangement in the 2007 runs was considered to be an adequate compromise between rate and signal size. If the SPS spill is eventually synchronized with the LHC clock and the clock becomes available at the H2 test beam area, the need for a trade-off between event rate and signal size will disappear.

In summer 2007 runs, NIM logic modules were used to form the trigger based on the coincidence of two scintillation counters. The active area of the scintillators was larger than the active area of the SiBT [2]. Unlike the reference and test modules, the scintillation counters were not rotated. Thus, particle tracks crossing corners of the scintillator counters did not necessarily pass through the active regions of the modules. Similarly, particle tracks crossing the extreme corners of the detector modules did not necessarily pass though the counters. Figure 4 illustrates the different regions.

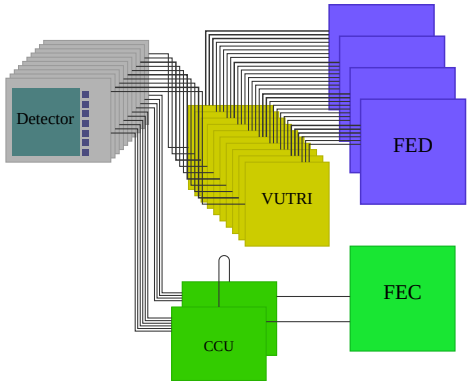

Fig. 5. The FEC communicates with the CCU's through a token ring and the CCU's exchange information with the individual hybrids via the I^2C protocol. The flow of data from the hybrids to the FED's is described in the text.

5. Readout

The SiBT data acquisition (DAQ) is based on prototypes of the CMS data acquisition hardware: PCI Mezzanine Card (PMC) based Front End Controller (FEC) and Front End Driver (FED) boards, and a TSC.

The SiBT DAQ system communicates with the front end chips through an electrical version of the FEC [22] card and the Communication and Control Unit (CCU25) [23] IC. One FEC and two CCU's are needed to communicate with the 10 hybrids used in the SiBT (Fig. 5). The FEC is used to distribute clock and trigger information from TSC to the front end chips, to set the tunable parameters of the front

[2] With perfect alignment the common area of the counters would have been about $50 \times 50\,\mathrm{mm}^2$. This was larger than the $\sim 38 \times 38\,\mathrm{mm}^2$ overlap region in the telescope. Fiducial cuts further reduce the detector overlap area by about 10%. See Fig. 10.

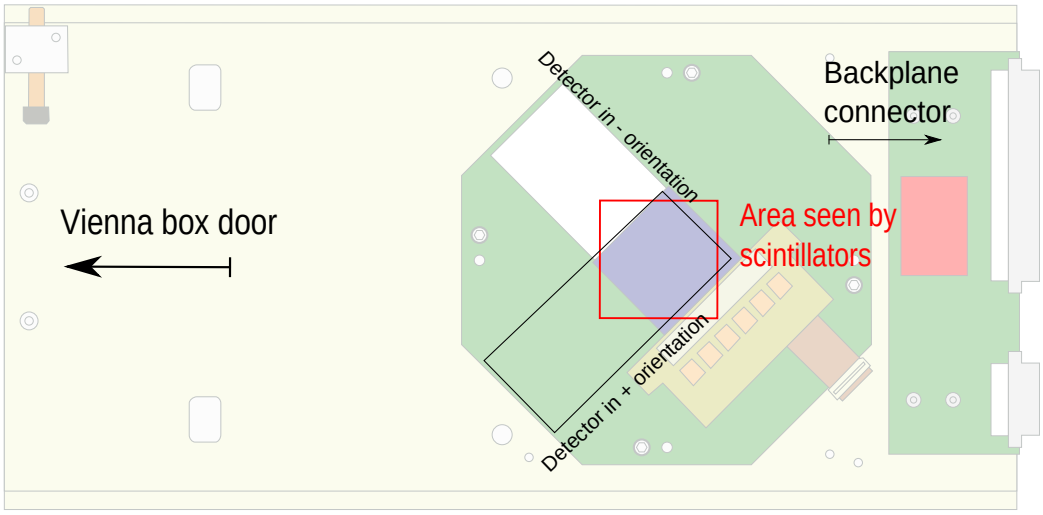

Fig. 4. Reference detector and superimposed active triggering area. For a flat beam spatial distribution, 58% of the triggered events should contain a track within the active area. The detectors were mounted with ± 45° rotations since the vertical clearance of the Vienna box did not allow a 90° orientation. The figure clarifies the + and − detector orientations described in the text.

end chips, and optionally to read operating parameters from the Detector Control Unit (DCU) [18]. The actual measurement data is transmitted through differential current signals from the front end chips to APVMUX ASIC, from APVMUX to VUTRI cards in multiplexed differential voltage signals, and finally from VUTRI's to FED [24] cards after being further amplified in the VUTRI cards.

The FED's require clock and trigger signals from the TSC to be able to record measurement data from the front end. After the FED has received a trigger, it will detect the incoming APV frames and digitize them. The non-optical version of the CMS FED does not support sparcification, so that all channels are read out for each event (*virgin raw* mode [3]). Also, each electrical FED can read out the data only from eight APV pairs. Since there were 5 active APV's per reference module, three FED's were needed to read out the 3×8 APV pairs from the eight reference detectors and a fourth FED was required for reading out the module or modules under study.

Unlike the CMS module burn-in DAQ system, which relied on multiplexing to read up to 10 modules, the SiBT DAQ has to read up to 10 modules simultaneously. In order to accomplish this with the older CMS electronics it was necessary to use four computers at the same time. Three of the computers were of the same vintage as the older data acquisition hardware in order to avoid compatibility issues. Each of the three older PC's housed two DAQ PCI boards for a total of six PCI boards. Limiting the number of PCI boards per computer was necessary to insure sufficient ventilation. The fourth computer, currently a 2.8 GHz Intel Pentium 4 PC executes the CPU intensive parts of the online software.

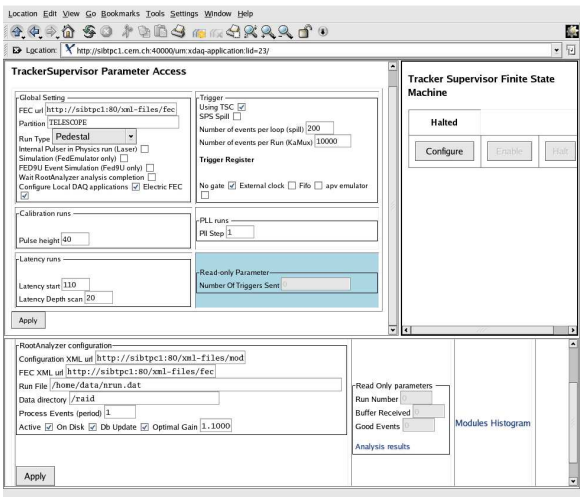

Fig. 6. The data acquisition is controlled through dynamic web pages.

[3] The FED can also record data in a trigger-less mode (so called *scope mode*), but this mode is not suitable for data acquisition. The final versions of the FED support other data acquisition modes in addition to the two mentioned here.

6. Software

The upgraded SiBT used an early version of the CMS XDAQ-based readout software [25]. The latest versions of the online software make hardware related assumptions which are not compatible with the prototype boards. The selected software, rc1205, is written in C and C++ programming languages on top of the XDAQ framework. It dates back to December 2005 and had been prepared for the CMS module testing centers during the construction phase. It took considerable effort to get the code to function in the test beam setup. However, with the necessary modifications the software ran well in the beam tests. The program flow of this software package is very similar to that which is described in the CMS Technical Design Report [26].

The rc1205 application starts out by launching XDAQ programs on each of the four Linux computers. The XDAQ executives are then configured by a *HyperDAQ* [27] interface using a web browser or, alternatively, through SOAP messaging. As a part of configuration, XDAQ loads and starts the data acquisition applications. The DAQ applications acquire their configuration in XML format via the HTTP protocol.

The data acquisition procedure is controlled by *TrackerSupervisor* application. There are several modes of operation available, and the device can auto-calibrate, i.e., obtain needed timing and pedestal values for itself. Some calibration steps must be done manually since the integrated calibration procedure makes hardware assumptions that were not met by the upgraded SiBT. With the exception of the startup procedure, the SiBT operator can carry out all of the steps required for a data run through a web browser interface (Fig. 6).

In addition to its asynchronous nature (relative to the SiBT DAQ) the H2 beam also contained a macro structure. That is, particles were available for only a fraction (typically ∼15%) of each SPS supercycle [28]. The data acquisition software in the 2007 runs did not take advantage of this structure (Fig. 7), although this is envisioned for future runs. In the 2007 configuration the deadtime was approximately 7.3 ms per event. The spill structure and readout related deadtime limit the SiBT event rate to approximately 25 Hz. The exact upper limit depends on the actual SPS spill cycle [4].

[4] The SPS spill cycle length was changed several times during the summer 2007 test run period.

Some modifications to the rc1205 code were either necessary or desirable for use with the beam telescope. These included changes necessitated by the older hardware, changes to allow the operator to monitor program flow and run progress, and a change to implement autologging. The autologging included information from the DAQ software such as the run number, timestamps for the beginning and end of a run, the number of events, and values of operator modifiable parameters. In addition to these changes, all configuration file changes were logged and timestamped, so that a complete set of information is retrievable for each run.

In addition to rc1205 code, the SiBT setup also utilized some software that is not part of the CMS online software, such as the program used for reading out the Vienna box temperature sensors.

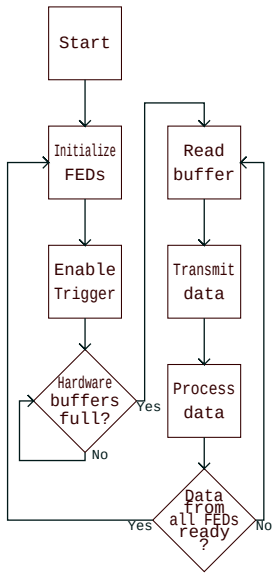

Fig. 7. A simplified diagram of the program flow during data acquisition. The FED buffers are emptied sequentially during the spill.

7. Results

The analysis of SiBT data proceeds along conventional lines. First, a special, non-beam run is taken to determine the average ADC level (pedestal) and its standard deviation (N_s) for each individual strip. These values are then used to define clusters in the beam data, and the centroids of the clusters formed the inputs to a straight line track fitting algorithm. The ultimate goal of the tracking is to determine the intersection of a 3D track with the detectors under

study, and to use this information to measure hit resolution and efficiency.

In Table 1 we list S/N values for reference detectors from the summer 2007 running period. These values are calculated in a similar way as in Ref. [11]. Here $S = S_C = \sum S_s$, but N is taken as the average noise level of an individual strip ($N = \sqrt{\frac{1}{n}\sum N_s^2}$) instead of the cluster noise N_C. These results agree with the expected value of 30 for the combination of the reference sensors and the APV25S1 chip [14,19]. The S/N values are slightly higher than the values of the previous SiBT setup, even though the strips are now longer.

Table 1
Key parameters for SiBT detectors. Detector numbers are as in Fig. 3. The cluster signal-to-noise ratio S/N, efficiency $\varepsilon_{3\sigma}$ and detector resolution σ_m are computed only for reference detectors. The impact point error σ_f is computed also for the detector under study.

Det #	S/N	$\varepsilon_{3\sigma}$ (%)	σ_f (μm)	σ_m (μm)
1	28.4	93.4	6.7	8.4
2	28.6	95.1	5.8	8.3
3	28.0	94.0	5.1	8.4
5	28.8	94.8	4.2	8.3
6			4.2	
7	28.4	93.8	4.5	8.1
8	29.0	94.2	5.1	8.4
9	28.7	94.7	5.8	8.4
10	28.2	94.0	6.7	8.4

Based on the individual pedestal and noise values cluster candidates were constructed around peak strips as defined by $S_s/N_s > 4$. All adjacent strips with $S_s/N_s > 3$ were added to the cluster. In case no such neighboring strips were found, the nearest neighboring strips were added provided that their S_s was positive. Cluster candidates were accepted if $S_C/N_C > 5$. Here the cluster signal is $S_C = \sum S_s$ and the cluster noise is $N_C = \sqrt{\sum N_s^2}$, both summed over the strips of the cluster.

The exact position of a hit was calculated from the charge-sharing of the peak strip and the neighboring strips. A hit from all reference detectors was required for a track. A χ^2 cut of 10 was used. Detector resolutions σ_m were iteratively calculated as $\sigma_m = \sqrt{\sigma_r^2 + \sigma_f^2}$ [29], where σ_r is the σ of a Gaussian fitted to the residual distribution and σ_f is the impact point error as defined below. A typical residual distribution is shown in Fig. 8.

The resolutions σ_m are given in Table 1. They are slightly better than the digital resolution of $\frac{p}{\sqrt{12}} = 8.7\,\mu$m, where p is one half of the nominal readout pitch. This suggests that intermediate strips effectively double the number of strips, at least as far as resolution is concerned.

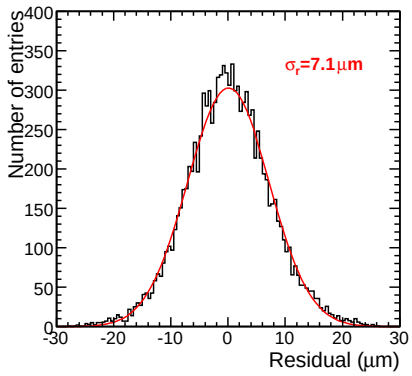

Fig. 8. Residual distribution of detector 5 and the fitted Gaussian.

Detector resolutions σ_m were used iteratively to calculate the measurement precision for tracks (the impact point error σ_f). The method of ref. [30] was followed, and zero magnetic field and negligible multiple scattering were assumed. For the mid-point of the Vienna box, the impact point error was found to be $\sigma_f = 4.2\ \mu$m. The variation of the impact point error within the Vienna box is illustrated in Fig. 9 and explicit values are given in Table 1.

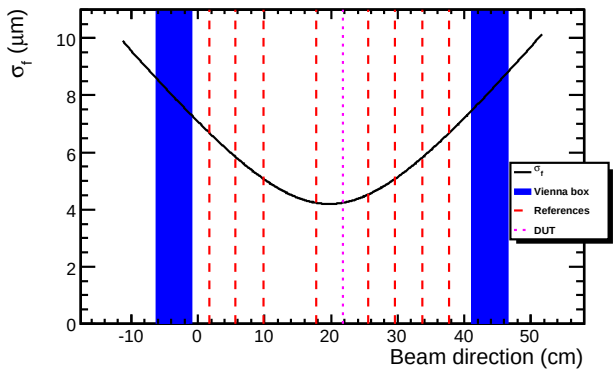

Fig. 9. Theoretical measurement resolution of tracks (impact point error) calculated from the measured detector resolutions. The measurement direction of detectors in + orientation is shown.

The detector efficiency $\varepsilon_{3\sigma}$ was calculated in a separate analysis by excluding the detector in question from the track fit, and checking if a cluster was found

in a neighborhood of $3\sqrt{\sigma_m^2 + \sigma_f^2}$ of the track [10]. This size of the search window corresponds to the χ^2 cut of the track fit.

Efficiencies $\varepsilon_{3\sigma}$ of individual reference detectors are given in Table 1. The obtained values of 93–95% are smaller than the values typically reported, which are of the order of 99%. One possible reason for low efficiencies is that there was no possibility to optimize the running parameters of DAQ during operation of SiBT.

Reference detectors could successfully measure 56% of triggered tracks in the run 605 from June 2007. This corresponds roughly to the geometrical acceptance shown in Fig. 4. The beam profile (Fig. 10) was such that approximately half of the effective area of the reference detectors was exposed to an intensity exceeding half of the maximum intensity of the beam. A hit from all reference detectors was required for a track in the analysis run. Thus, a poorly performing readout chip would have deteriorated efficiency in a rectangular area of 0.8×3.8 cm^2 along the strip direction. Therefore Fig. 10, together with other similar plots and performance plots of individual detectors, strongly suggests that all readout chips were working properly.

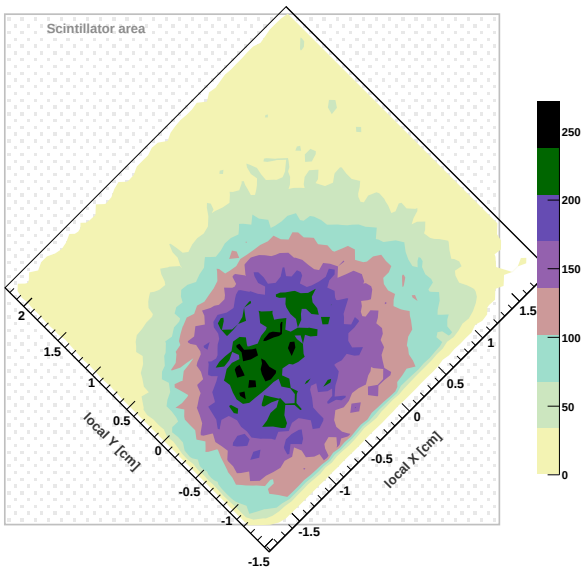

Fig. 10. Beam profile at slot 6 in run 605. The acceptance region for tracks in the local Y direction (corresponding to the − orientation) is slightly smaller than in the X direction due to the misalignment of some of the Y detectors. Projection of scintillator area is shown for illustrative purposes, and has not been accurately measured.

8. Future Improvements

The SiBT upgrade in 2007 was a nearly complete rebuild of the system. The new SiBT was able to record tracks from day one. The first tests demonstrated that a faster event rate and a larger temperature range would further extend the usability of the SiBT.

The rate of recorded events in which tracks are reconstructed was currently limited by the trigger geometry. Improving the trigger efficiency (by rotating the beam counters to match the sensor orientations) would increase the track rate close to the trigger rate. This maximum rate is limited by system deadtime. Modifying the state machine of the online acquisition loop (Fig. 7) would reduce the system deadtime by at least one order of magnitude. This would require additional code changes in several XDAQ executives in the already modified rc1205 release.

In the beam tests discussed in this paper, the Vienna box Peltier elements used room temperature water for cooling. Pre-cooling the water would increase the cooling power of the system. It should also be possible to implement a mechanism which would allow the resetting of the PLL's in case of a lockup. By implementing both of these improvements it should be possible to achieve a much lower operating temperature in future operations of the SiBT.

The autologging feature of the SiBT could be extended to automatically store the detector bias parameters, which are retrievable from the SY127 power supply.

9. Conclusions

The SiBT provides a means of probing the cluster resolution, signal-to-noise, and charge collection efficiency properties of silicon microstrip detectors. The beam telescope is particularly useful as it facilitates the measurement of both depletion voltage and hit resolution for irradiated and non-irradiated sensors in a common setting. In the 2007 implementation of the SiBT, the reference track position was measured with an accuracy of 4 μm. This value is more than adequate to probe the hit resolution of the smallest pixel and strip pitches under consideration for S-LHC experiments. The SiBT collaboration expects to continue the study of radiation-hard sensor candidates, such as MCz silicon, in test beam

operations during the summer of 2008.

10. Acknowledgements

We wish to express our thanks to the DØ collaboration for the Run IIb sensors for the SiBT reference plane modules and to Dr. Laurent Mirabito for the XDAQ rc1205 software release. In addition, we would like to thank Dr. Dragoslav-Laza Lazic and the CMS HCAL collaboration for their valuable technical assistance and co-operation at the CERN H2 experimental area. This work has partially been funded by the Academy of Finland. These results have been obtained in the frameworks of CERN CMS and RD50 collaborations.

References

[1] RD50 Status Report 2006, CERN-LHCC-2007-005.
[2] J. Härkönen et al., Nuclear Instruments & Methods in Physics Research A 514 (2003) 173–179.
[3] Zheng Li et al., Nucl. Inst. & Meth. A A 579 (2007) 775–781.
[4] G. Casse, Nucl. Inst. & Meth. A 579 (2007) 623–627.
[5] A. Roy et al., Nucl. Inst. & Meth. A 552 (2005) 112–117.
[6] E. Verbitskaya et al., Nucl. Inst. & Meth. A, 583 (2007) 77–86.
[7] G. Kramberger and D. Contarato, Nucl. Inst. & Meth. A 560 (2006) 98–102.
[8] M.Moll, et al., Development of radiation tolerant semiconductor detectors for the Super-LHC, Nucl. Inst. & Meth. A 546 (2005) 99–107.
[9] E. Tuominen et al., IEEE Transactions in Nuclear Science 50 (1) (2003) 1942–1946.
[10] I. Hietanen et al., Nucl. Inst. & Meth. A 310 (1991) 677–680.
[11] C. Eklund et al., Nucl. Inst. & Meth. A 430 (1999) 321–332.
[12] M. Meschini et al., Nucl. Inst. & Meth. A 447 (2000) 133–141.
[13] C. Bozzi, CMS NOTE 1997/026.
[14] M.Raymond et al., The 6th workshop on electronics for LHC experiments, Krakow, Sept. 2000.
[15] M. French et al., Nucl. Inst. & Meth. A 466 (2001) 359–365.
[16] F. Beißel et al., IEEE Transactions on Nuclear Science 52 (6) (2005) 3199–3205
[17] Documents 314986/1, 314987/1, 314983/1, 318639/5, 318642/5 and 318641/5, CERN engineering data management service.
[18] G. Magazzu et al., DCUF User Guide, CERN EP/MIC, 2003.
[19] M. Demarteau et al., DØ note (2003) 4308.
[20] M.Axer et al., CMS NOTE 2005/020.
[21] M.Ageron, Trigger Sequencer Card User Manual, IPNL Lyon 2001.
[22] F. Drouhin et al. 2004 IEEE Nuclear Science Symposium Conference Record IEEE Cat. No. 04CH37604. 2004: Vol. 2, 1196–1200.
[23] C. Paillard et al., 8th Workshop on Electronics for LHC Experiments, Colmar, France, 9–13 Sep. 2002, 174–178.
[24] S.A. Baird et al., IEEE Real-Time Conference, Santa Fe, USA, June 1999.
[25] J. Gutleber, L. Orsini, Cluster-Computing 2002 5(1), 55–64, Kluwer Academic Publishers.
[26] The CMS Tracker Project Technical Design Report CERN/LHCC 98-6.
[27] R. Arcidiacono et al., Where Data Acquisition Meets The Web, 10th ICALEPCS Int. Conf. on Accelerator and Large Expt. Physics Control Systems, Geneva 2005.
[28] R.J. Lauckner, Pulsed operation of the CERN SPS collider, 11th Particle Accelerator Conference : Accelerator Engineering and Technology, pt. 1, Vancouver, Canada, 13–16 May 1985, 1653.
[29] K. Banzuzi et al., Nucl. Inst. & Meth. A 453 (2000) 536–544.
[30] V. Karimäki, CMS NOTE 1997/064.